RSC Advances

ROYAL SOCIETY OF CHEMISTRY

www.rsc.org/advances

Fabrication of heterostructured Ag/AgCl/Bi_2MoO_6 plasmonic photocatalyst with efficient visible light activity toward dye

Qing Yan,[a] Meng Sun,*[a,b] Tao Yan,[a] Mengmeng Li,[c] Liangguo Yan,[a] Dong Wei[a] and Bin Du*[a]

[a] School of Resources and Environment, University of Jinan, Shandong Provincial Engineering Technology Research Center for Ecological Carbon Sink and Capture Utilization, Jinan 250022, P.R. China. Fax: +86 531-82765969; Tel: +86 531-82769235; E-mail: smlcu@163.com, bindu61@gmail.com

[b] Fujian Provincial Key Laboratory of Photocatalysis-State Key Laboratory Breeding Base, FuzhouUniversity, Fuzhou 350002, P.R. China

[c] School of Civil Engineering and Architecture, University of Jinan, Jinan 250022, P.R. China.

Graphical abstract

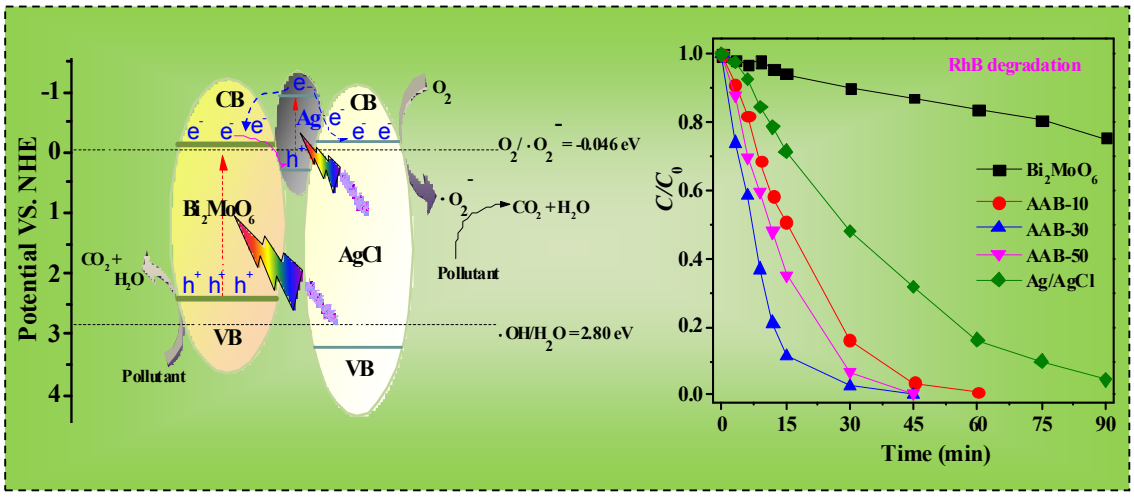

Cite this: DOI: 10.1039/c0xx00000x

www.rsc.org/xxxxxx

ARTICLE TYPE

Fabrication of heterostructured Ag/AgCl/Bi_2MoO_6 plasmonic photocatalyst with efficient visible light activity toward to dye

Qing Yan,[a] Meng Sun,*[a,b] Tao Yan,[a] Mengmeng Li,[c] Liangguo Yan,[a] Dong Wei[a] and Bin Du*[a]

Received (in XXX, XXX) XthXXXXXXXXX 20XX, Accepted Xth XXXXXXXXX 20XX

DOI: 10.1039/b000000x

Abstract: A ternary Ag/AgCl/Bi_2MoO_6 plasmonic photocatalyst was successfully fabricated through a two-step synthesis method. The obtained samples were characterized by X-ray diffraction (XRD), scanning electron microscope (SEM), transmission electron microscopy (TEM), and ultraviolet-visible diffuse reflectance spectroscopy (DRS). The DRS results showed that the visible light absorption of Ag/AgCl/Bi_2MoO_6 composite had been greatly enhanced owing to the surface plasmonic resonance (SPR) of Ag^0 particles. The SEM and TEM images showed that the obtained flower-like Bi_2MoO_6 microspheres were composed of nanoplates, on the surface of which Ag/AgCl particles were distributed. In the photocatalytic degradation of dyes, Ag/AgCl/Bi_2MoO_6 photocatalysts exhibited significantly enhanced activities compared with Bi_2MoO_6. It was also found that the components of Ag/AgCl/Bi_2MoO_6 have great influences on the activities. Controlled experiments proved that the degradation of pollutants over Ag/AgCl/Bi_2MoO_6 was mainly ascribed to the strong oxidation ability of photo-generated holes. On the basis of band structure analysis and active species trapping experimental results, a photocatalytic mechanism is also proposed.

Introduction

In the past many years, the water pollution problem becomes more and more severe because of the rapid development of industrialization and urbanization. The organic pollutants in contaminated wastewater were usually found to be toxic synthetic dyes, which are harmful to the environment and human health. Thus, great efforts have been done to explore green and economic methods for treating the organic pollutants discharged into the environment. For example, numerous researches have been focused on the photocatalytic degradation of stable organic pollutants,[1-4] which was difficult to remove using traditional treatment method. TiO_2, as an efficient photocatalyst, has been widely studied and applied in photocatalysis field because of its unique surface structure characteristics, high chemical stability, nontoxicity, and prefect photocatalytic activity.[5-8] However, its wide band gap (3.2 eV for anatase TiO_2) and low quantum efficiency have greatly hindered its practical application.[9-11] Therefore, it is an urgent topic to develop visible-light driven photocatalysts for the practical utilization of solar energy.

[a]*School of Resources and Environment, University of Jinan, Shandong Provincial Engineering Technology Research Center for Ecological Carbon Sink and Capture Utilization, Jinan250022, P.R. China. Fax: +86 531-82765969; Tel:+86 531-82769235;E-mail:smlcu@163.com, bindu61@gmail.com*

[b]*Fujian Provincial Key Laboratory of Photocatalysis-State Key Laboratory Breeding Base, Fuzhou University, Fuzhou 350002, P.R. China*

[c]*School of Civil Engineering and Architecture, University of Jinan, Jinan250022, P.R. China.*

Recently, noble metals with localized surface plasmonic resonance property have attracted considerable attention because of their strong absorption of visible light.[12-15] Among of which, Ag/AgCl-based composites have exhibited the most outstanding photocatalytic activity and stability.[16,17] Huang et al reported the synthesis of Ag/AgCl photocatalyst using ion-exchange method, which exhibited efficient activity for the degradation of methyl orange.[18] In order to further improve its activity, many researchers have focused on the morphology-controlled fabrication of Ag/AgCl.[16,19] Therefore, many Ag/AgCl-based hierarchical nanostructures, such as Ag/AgCl/WO_3,[20] AgCl/Ag/-TaON,[21] and Ag/AgCl/ $Bi_{20}TiO_{32}$,[22] have been fabricated and exhibited efficient activity. Furthermore, Ag/AgCl has also been successfully used to combine with flower-like semiconductors, such as Bi_2WO_6 [23] and BiOBr[24], and the photocatalytic activity has been greatly improved by the synergy effect of SPR effect driving from Ag nanoparticles and light scattering effect driving from flower-like structure.

In this work, Ag/AgCl has also been used to couple with a flower-like Bi_2MoO_6 photocatalyst via a two-step route. Bi_2MoO_6, with a narrow band gap of 2.5-2.8 eV, has been reported as an excellent photocatalyst from the viewpoint of utilizing visible light. It could serve as a solar-energy-conversion material for water splitting and the decomposition of organic compounds under visible-light irradiation.[25-27] Unfortunately, the rapid recombination of electrons and holes after photo-excitation leads to the low efficiency of Bi_2MoO_6. Thus, it was used to couple with Ag/AgCl to enhance the visible light responsive photocatalytic activity. The obtained Ag/AgCl/Bi_2MoO_6

composites have exhibited efficient activities in photocatalytic decomposing of Rhodamine B (RhB) dye under visible light illumination. After 40 min of reaction, the degradation ratio of RhB was up to 99%. The activity improvement should be ascribed to the SPR effect of Ag^0 and the formation of heterojunction, which respectively improved the visible light absorption and separation efficiency of photo-generated carriers.

Experimental section

Synthesis of flower-like Bi_2MoO_6 microspheres

All chemical reagents were analytical grade and used without further purifications. For the synthesis of flower-like Bi_2MoO_6 microspheres, 2 mmol of $Bi(NO_3)_3{\cdot}5H_2O$ and 1 mmol of $(NH_4)_6MoO_4{\cdot}4H_2O$ were dissolved in 20 ml of ethylene glycol and stirred for 120 min. Then 50 mL of ethanol was added into it. The mixture was stirred for another 10 min. The resulting solution was transferred into a 100 mL Teflon-lined stainless steel autoclave and kept at 160 ˚C for 12 h. Subsequently, the autoclave was cooled to room temperature naturally. The obtained samples were filtered, washed with deionized water for several times, and finally dried at 80 ˚C in air.

Synthesis of heterostructured Ag/AgCl/ Bi_2MoO_6 composites

In a typical synthesis of Ag/AgCl/Bi_2MoO_6 composites, 0.4 g of Bi_2MoO_6 powders and 0.075 g of hexadecyltrimethy-lammoniumchloride (CTAC) were added into 200 mL of deionized water and stirred for 60 min. Then 2.0 mL of 0.1 M $AgNO_3$ was quickly added into the above mixture. During this process, the excessive surfactant CTAC adsorbed onto the surface of Bi_2MoO_6 and induced Cl^- to react with Ag^+ to produce AgCl particles in the suspension. After 60 min of continuous stirring, the resulting suspension was then exposed to UV-vis light emitted by a 300 W Xe lamp for a certain time to deoxidize Ag^+ to Ag^0 on the surface of AgCl particles. The suspension was filtered, washed with deionized water, and dried at 80 ˚C for 12 h. The illumination time has great influence on the reduction of Ag^+, the obtained samples illuminated for 10, 30, and 50 min were marked as AAB-10, AAB-30, and AAB-50, respectively.

Characterization of photocatalysts

X-ray diffraction (XRD) patterns of the obtained products were recorded on a Bruker D8 Advance X-ray diffractometer under the conditions of generator voltage = 40 kV; generator current = 40 mA; divergence slit = 1.0 mm; Cu Kα (λ = 1.5406 Å). The morphologies and microstructures were examined with a Hitachi S-4800 scanning electron microscopy (SEM). The transmission electron microscopy (TEM) and high-resolution transmission electron microscopy (HRTEM) images were measured by a JEOL model JEM 2010 EX instrument at an accelerating voltage of 200 kV. Carbon-coated copper grid was used as the sample holder. The ultraviolet-visible diffuse reflectance spectroscopy (DRS) were measured at room temperature in the range of 200–700 nm on a UV–vis spectrophotometer (Cary 500 Scan Spectrophotometers, Varian, and U.S.A) equipped with an integrating sphere attachment. X-ray photoelectron spectroscopy (XPS) analysis was conducted on an ESCALAB 250 photoelectron spectroscopy (Thermo Fisher Scientific) at 3.0 × 10^{-10} mbar using Al Kα X-ray beam (1486.6 eV).

Evaluation of photocatalytic performance

Photocatalytic reactions were conducted in a customized reactor. The visible light photocatalytic activity of Ag/AgCl/Bi_2MoO_6 composites were evaluated by the degradation of dyes, A 300 W xenon lamp (PLS-SXE300C, Beijing Perfect Light Co. Ltd., Beijing) with two cutoff filters (420 nm < λ < 800nm) has been used as light source. In each experiment, 100 mg of photocatalyst was added into 100 mL of RhB dye aqueous solution (2 × 10^{-5} M). Before irradiation, the suspensions were magnetically stirred in dark for 60 min to ensure the establishment of an adsorption/desorption equilibrium between the photocatalyst and dye. During reaction under visible light irradiation, 3 mL of suspension was sampled and centrifuged to remove the photocatalyst particles at given time intervals. The resulting clear liquor was analyzed on a Perkin-Elmer UV-vis spectrophotometer (Model: Lambda 35) to record the concentration changes of dyes. The percentage of degradation is reported as C/C_0. C is the absorption of RhB absorption spectrum at 554 nm. And C_0 is the absorption of the starting concentration when adsorption-desorption equilibrium is achieved.

Results and discussion

Structural characterization

Figure 1 shows the XRD patterns of the obtained Bi_2MoO_6, Ag/AgCl and Ag/AgCl/Bi_2MoO_6 photocatalysts. As we can see, all the diffraction peaks of the obtained Bi_2MoO_6 sample located at 10.9, 23.6, 28.2, 32.5, 36.0, 46.8, 55.4, and 58.4° can be assigned to orthorhombic-phase Bi_2MoO_6 (JCPDS No. 76-2388). No impurity has been detected from the diffraction patterns. For the obtained Ag/AgCl sample, five characteristic diffraction peaks located at 27.8, 32.2, 46.2, 54.8, and 57.5◦ have been observed, which indexed to the (111), (200), (220), (311), and (222) planes of cubic phase AgCl (JCPDS No. 31-1238). In addition, a very weak diffraction peak of cubic phase Ag (JCPDS No. 65-2871) located at 38.1◦ has also been observed, this result was in accordance with the experimental phenomena that the color of AgCl changed from white to gray during light irradiation. As for the Ag/AgCl/Bi_2MoO_6 photocatalysts, it is difficult to distinguish which diffraction peak was ascribed to Ag/AgCl or Bi_2MoO_6 because of the overlapping of their main diffraction peaks (See Figure 1).

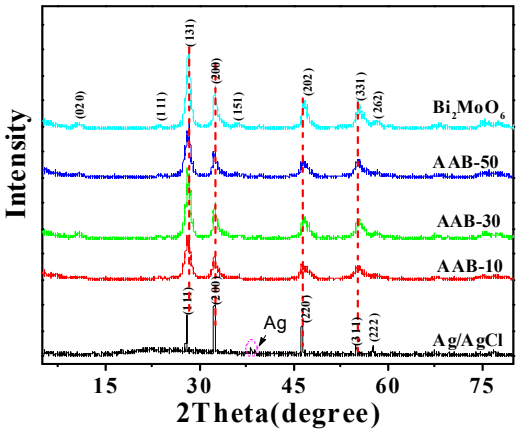

Figure 1. XRD patterns of pure Bi_2MoO_6, Ag/AgCl, and Ag/AgCl/Bi_2MoO_6 composites.

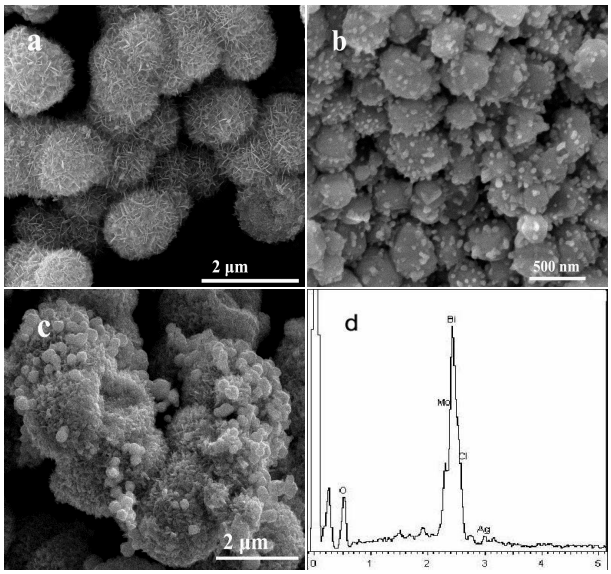

Figure 2. SEM images of the as-prepared sample: (a) pure Bi_2MoO_6, (b) Ag/AgCl, (c) Ag/AgCl/Bi_2MoO_6 composite, and (d) corresponding EDX spectrum for Ag/AgCl/Bi_2MoO_6 composite.

Morphology and microstructure

The morphologies of Bi_2MoO_6, Ag/AgCl and Ag/AgCl/Bi_2MoO_6 composites have been characterized by SEM. Fig. 2a shows that the obtained Bi_2MoO_6 exhibited flower-like microsphere morphology. The microspheres with average diameter of 1-2 μm were composed of large amount of nanoplates. Meanwhile, Fig. 2b shows that the obtained Ag/AgCl exhibited particle morphology with smaller sizes of 400-500 nm compared with Bi_2MoO_6. Even smaller Ag nanoparticles (average diameter of 50 nm) have also been observed on the surface of AgCl. Fig. 2c shows that when Ag/AgCl was coupled with Bi_2MoO_6, the Ag/AgCl particles would be decorated on the surfaces of flower-like Bi_2MoO_6 structures. The element composition of the Ag/AgCl/Bi_2MoO_6 composites has been measured using energy-dispersive X-ray (EDX) spectroscopy, and the corresponding result was shown in Figure 2d. It shows that the composites are mainly consisted of Bi, O, Mo, Cl, and Ag elements.

The morphology and nanostructures of Ag/AgCl/Bi_2MoO_6 composite were further investigated by TEM and HRTEM. Fig. 3a shows that the Ag/AgCl/Bi_2MoO_6 composite possessed microsphere morphology, and the average diameter of the microspheres was about 1.5 μm. The HRTEM image showing clear lattice planes was shown in Figure 3b. The uniform fringe with an interval of 0.327 nm was indexed to the (140) facet of Bi_2MoO_6. Another set of clear fringes with an inter-planer spacing of 0.277 nm corresponded to the (200) lattice plane of AgCl, while the fringe of 0.204 nm could be ascribed to the (200) facet of Ag. Figure 3b implies that obvious interfaces between Bi_2MoO_6 and Ag/AgCl can be observed. This result suggests that the heterojunction is actually formed at the interfaces of those materials. The elemental mapping has been performed to investigate the distribution of Ag/AgCl over Ag/AgCl/Bi_2MoO_6 composites. Figure 3 also displays the elemental mapping images for the Ag/AgCl/Bi_2MoO_6 sample. The cyan, red, and yellow-brown color of the images was respectively acquired at the K-

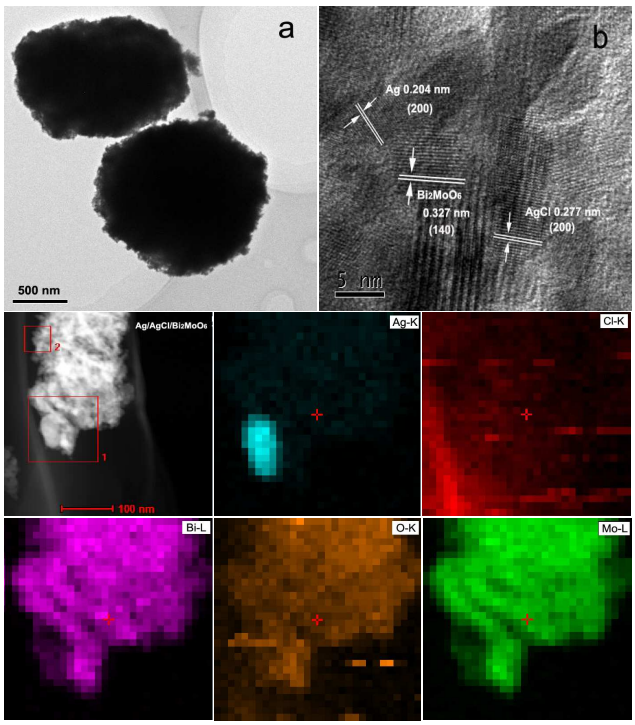

Figure 3. TEM and HRTEM images of the as-prepared sample: (a) TEM micrographs of Ag/AgCl/Bi_2MoO_6 composites, (b) HRTEM image of Ag/AgCl/Bi_2MoO_6 composites showing the formation of heterojunction structure, and corresponding elemental mapping images of Ag, Cl, Bi, O, and Mo elements.

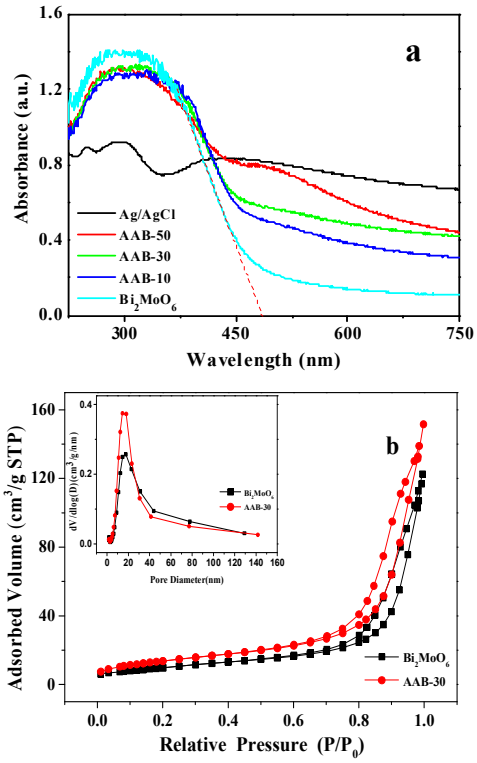

Figure 4. (a) UV–vis diffuse reflectance spectra of Bi_2MoO_6, Ag/AgCl, and Ag/AgCl/Bi_2MoO_6 composites. (b) N_2 adsorption–desorption isotherm and the pore size distribution plot for AAB-30 and Bi_2MoO_6. The pore size distribution was estimated from the desorption branch of the isotherm.

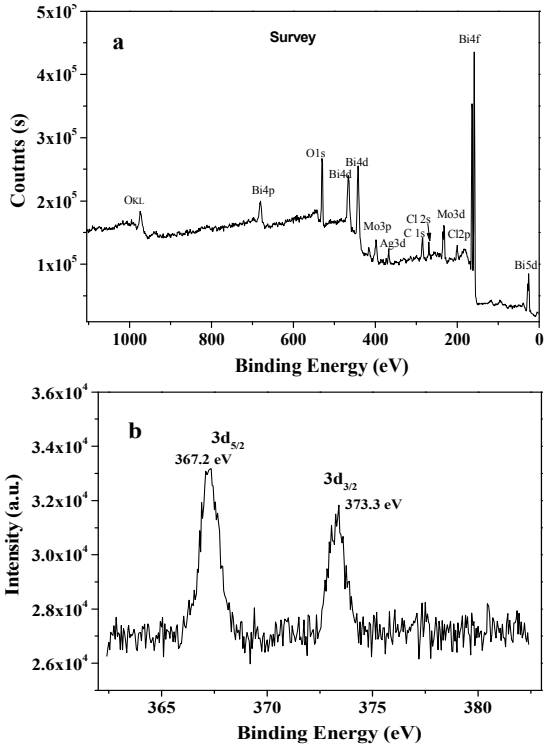

Figure 5. XPS spectra of Ag/AgCl/Bi_2MoO_6 photocatalys (a) survey spectrum and (b) Ag 3d.

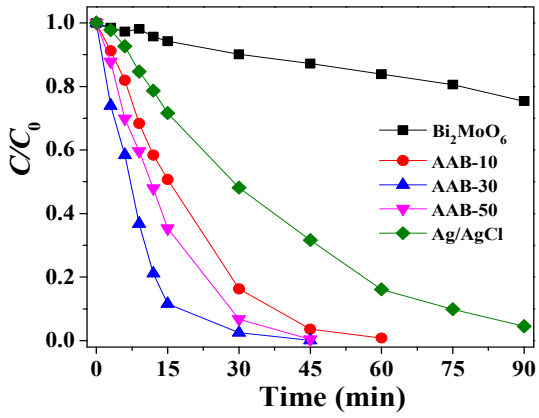

Figure 6. Degradation rates of RhB under visible light irradiation using Bi_2MoO_6, Ag/AgCl, and Ag/AgCl/Bi_2MoO_6 composites.

line spectra of Ag, Cl, and O elements, while that for the magenta and green color was respectively acquired at the L-line spectra of Bi and Mo elements. This result provides solid evidence that Ag/AgCl were successfully combined with Bi_2MoO_6.

DRS and BET surface analysis

The UV-vis diffuse reflectance spectra (DRS) have been performed to investigate the optical properties of the as-prepared samples. As shown in Figure 4a, the absorption edge of Bi_2MoO_6 was estimated to 485 nm showing a strong absorption in the UV range, while Ag/AgCl exhibited strong light absorption in the visible light region. When Ag/AgCl combined with Bi_2MoO_6, the absorption edges of Ag/AgCl/Bi_2MoO_6 composites were red-shifted. The visible light adsorption has also been greatly enhanced compared with pure Bi_2MoO_6. Figure 4b shows the nitrogen adsorption isotherm for the as-synthesized AAB-30 and

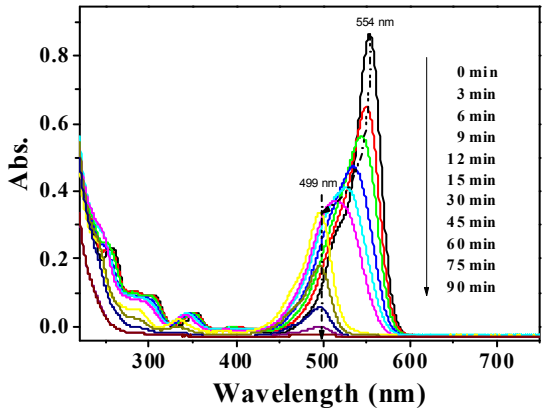

Figure 7. The absorption spectra of RhB in the presence of AAB-30 under exposure to visible light (420 nm < λ < 800 nm).

Bi_2MoO_6 sample, which exhibited the stepwise adsorption and desorption (type-IV isotherm). The pore-size distribution plot (inset) showed that the samples had exhibited a mean pore diameter of 16 nm with a narrow distribution of pore size. The BET specific surface area of AAB-30 was 50.4 $m^2 \cdot g^{-1}$, larger than that of Bi_2MoO_6 (35.7 $m^2 \cdot g^{-1}$).

XPS characterization

The XPS characterization was performed to investigate the chemical composition of Ag/AgCl/Bi_2MoO_6 sample and identify the chemical state of the Ag element. The results have been added into the revised manuscript. Figure 5a shows the XPS survey spectra of AAB-30 sample. As we can see, the sample contains Bi, Mo, O, Ag, Cl and C elements. The C element should be attributed to the adventitious hydrocarbon from the XPS instrument itself. Figure 5b shows that Ag 3d peak locates at the binding energy of 367.2 eV. Compared with that for bulk Ag (368.2 eV), it shows a peak shifts to the lower binding energy. Very similar phenomenon has also been reported [28-30], and the shift of the binding energy of Ag 3d should be primarily attributed to the interactions among the Ag, AgCl and Bi_2MoO_6.

Photocatalytic activity tests

To investigate the influences of Ag/AgCl on the photocatalytic activities, Ag/AgCl/Bi_2MoO_6 composites prepared under different conditions have been used to decompose RhB in water under visible light irradiation. Figure 6 shows the photocatalytic degradation results of RhB over pure Bi_2MoO_6, Ag/AgCl, and Ag/AgCl/Bi_2MoO_6 composites. As we can see, all of the Ag/AgCl/Bi_2MoO_6 composites have exhibited efficient activities, which were higher than that for pure Bi_2MoO_6 or Ag/AgCl. After 45 min of visible light irradiation, the degradation ratio of RhB over Ag/AgCl and Bi_2MoO_6 was only about 70 and 20%, respectively. As for the Ag/AgCl/Bi_2MoO_6 composites, the AAB-30 sample exhibited the best activity, and the degradation ratio of RhB was nearly to 100%. That is to say, the amount of Ag/AgCl has great influence on the photocatalytic activity. Figure 7 shows the temporal evolution of the spectral changes of RhB mediated by AAB-30. It exhibited that the absorption peak of RhB located at 554 nm gradually blue-shifted to 499 nm within 30 min of reaction. This hypsochromic shift of absorption maximum was caused by the N-deethylation of RhB during irradiation, which has been confirmed by Watanabe and co-

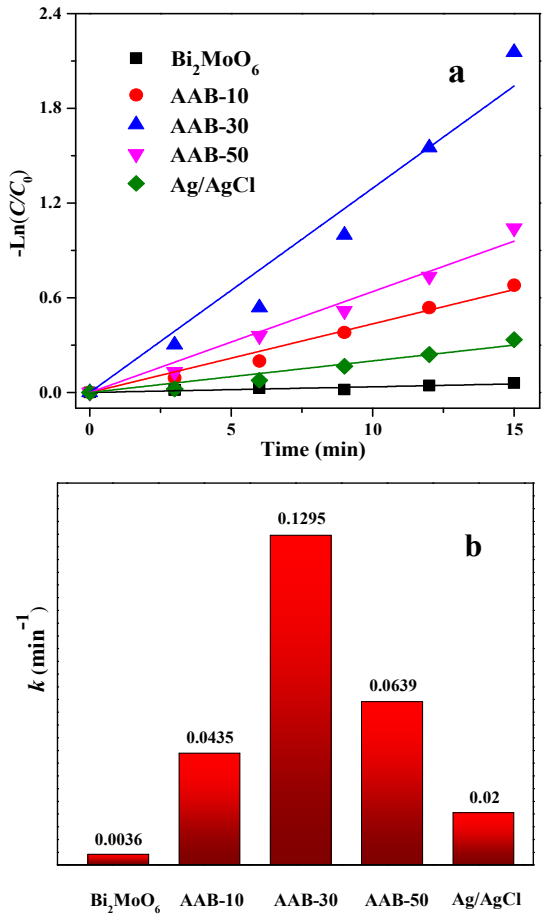

Figure 8. (a) plots of $-\ln(C/C_0)$ vs the irradiation time for RhB aqueous solution over different samples under visible light irradiation (420 nm < λ < 800 nm); (b) The kinetic constant k (min^{-1}) for different samples.

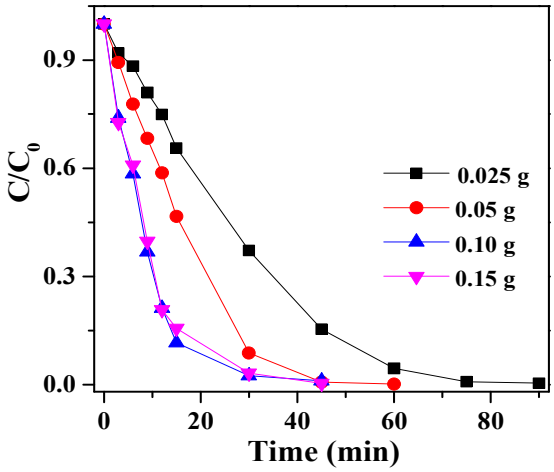

Figure 9. Photocatalytic degradation of RhB with different dosages of AAB-30 under the visible light (420 nm < λ < 800 nm) irradiation.

workers.[31,32] After that the peak decreased in the following degradation process and finally disappeared.

The reaction kinetics study shows that the photocatalytic degradation of RhB dye over those photocatalysts followed pseudo-first-order kinetic model. The rate constant (k) can be calculated by the formula of $-\ln(C/C_0) = k \cdot t$.[33] k is kinetic constant (min^{-1}), while t represents the irradiation time (min). Figure 8 showed the kinetic plots for RhB degradation over different photocatalysts. The rate constant of the photocatalytic degradation of RhB over AAB-30 photocatalyst is 0.1295 min^{-1}, which is much higher than that of Bi_2MoO_6(0.0036 min^{-1}), Ag/AgCl(0.0200 min^{-1}), or other Ag/AgCl/Bi_2MoO_6 composites (0.0435 and 0.0639 min^{-1} for AAB-10 and AAB-50, respectively). Thus, Ag/AgCl/Bi_2MoO_6 composite photocatalysts exhibited the enhanced photocatalytic activities, among of which AAB-30 was the most efficient. That is to say, the irradiation time played an important role in improving the activities, with too long or too short illumination time should be avoided. With a shorter illumination time as to 10 min, only a very small amount of Ag^0 would be produced over the sample, leading to weak light absorption ability and a lower activity. However, when the illumination time was longer than 50 min, too much of AgCl would be photo-reduced to form Ag/AgCl nano-clusters. The Ag/AgCl clusters might further agglomerated and shaded the active sties on the surface of Bi_2MoO_6.[34,35] Therefore, the degradation rates would be depressed accordingly.

Figure 9 showed the photocatalytic degradation of RhB at different dosages of AAB-30 photocatalyst under visible light irradiation. It was obviously that the degradation rate of RhB was accordingly improved when the amount of AAB-30 added was increased from 0.025 to 0.100 g, and nearly 100% of RhB has been decomposed within 30 min of reaction. The activity increased with photocatalyst concentration enhancement was a characteristic of heterogeneous catalysis. This phenomenon can be rationalized in relation to the amount of surface active cites as well as the light penetration into the suspensions.

The stability of a photocatalyst is very important for its practical application. In this work, Ag/AgCl/Bi_2MoO_6 composite photocatalyst was recycled for four times in the photocatalytic degradation experiments. Figure 10 showed the life-time test results. The photocatalytic activity of AAB-30 composite only deteriorated slightly in the reuse cycles. Figure 11 showed the XRD patterns of AAB-30 composites before and after RhB degradation. It illustrated that the crystal structure of the AAB-30 photocatalyst had not changed during the photocatalytic reaction. In order to study the degradation mechanism of RhB over AAB-30 photocatalyst, diagnostic experiments have also been performed with different active scavenger added. Herein, *tert*-butanol (TBA), p-Benzoquinone (PBQ), and oxalate was respectively used as hydroxyl radical, superoxide radical, and hole scavengers.[36,37] Figure 12 presented the influences of active species (such as ·OH, $\cdot O_2^-$, and h_{VB}^+) on the degradation rates of RhB. In the presence of AO (1.0 mL added), the peak blue-shift of RhB became very slow during the degradation process, meaning that the N-deethylation of RhB becoming more difficult. What was worse, the blue-shift absorption peak of RhB did not disappear after 90 min of reaction, but observed with relatively higher peak intensity. When PBQ was added into the system, a very similar situation was observed, but the degradation rate was further decreased. However, when certain amount of TBA was added into the system, it could hardly affect the N-deethylation process and degradation rates of RhB. That is to say, during the degradation process of RhB, $\cdot O_2^-$ and h_{VB}^+ played more important role compared with other active species.

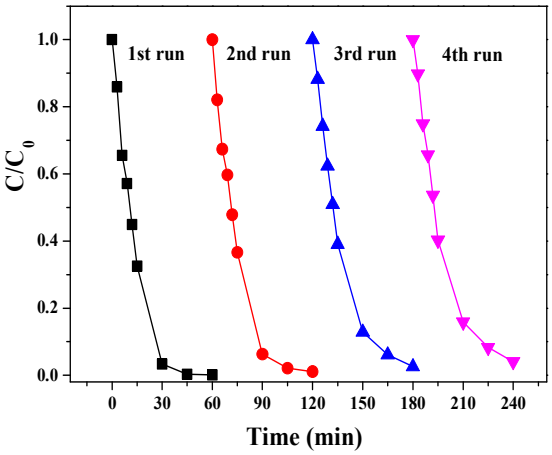

Figure 10. Photocatalytic performances of AAB-30 composite photocatalyst in the first four reuse cycles.

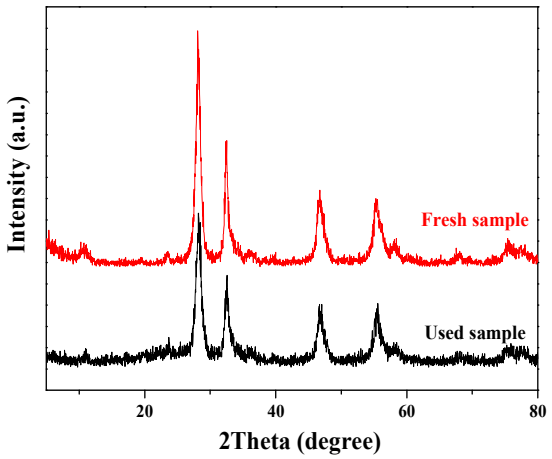

Figure 11. XRD patterns of AAB-30 before and after photocatalytic degradation of RhB.

As discussed above, $Ag/AgCl/Bi_2MoO_6$ composites have exhibited enhanced photocatalytic activity for decomposing RhB dye compared with pure Bi_2MoO_6. This activity enhancement should be ascribed to two main reasons, including their suitable band potentials and the SPR effect of Ag. According to the band gap structure of $Ag/AgCl/Bi_2MoO_6$ and the effects of scavengers, a possible pathway for the photocatalytic activity enhancement mechanism of $Ag/AgCl/Bi_2MoO_6$ photocatalyst was proposed (shown in Scheme 1). Bi_2MoO_6 possessed a band gap of 2.58 eV, and the conduction band (CB) and valence band (VB) energy levels are ca. -0.13 and 2.45 eV (vs NHE).[26] The positive potential endows the VB holes of Bi_2MoO_6 with high oxidation ability. That is to say, the holes generated over could directly react with pollutants absorbed on its surface. As for Ag/AgCl, it has been reported as an efficient visible light photocatalyst result in the strong surface plasmon resonance of metallic Ag^0 species. With a large band gap of 3.26 eV, AgCl cannot be excited by visible light, but its lower CB potential (−0.06 vs NHE) enabled the plasmon-induced electrons over Ag to transfer to the CB of AgCl.[26] On the other hand, metallic Ag specie could strongly absorb visible light because of its surface plasmon resonance effect, which was also beneficial for activity enhancement. The

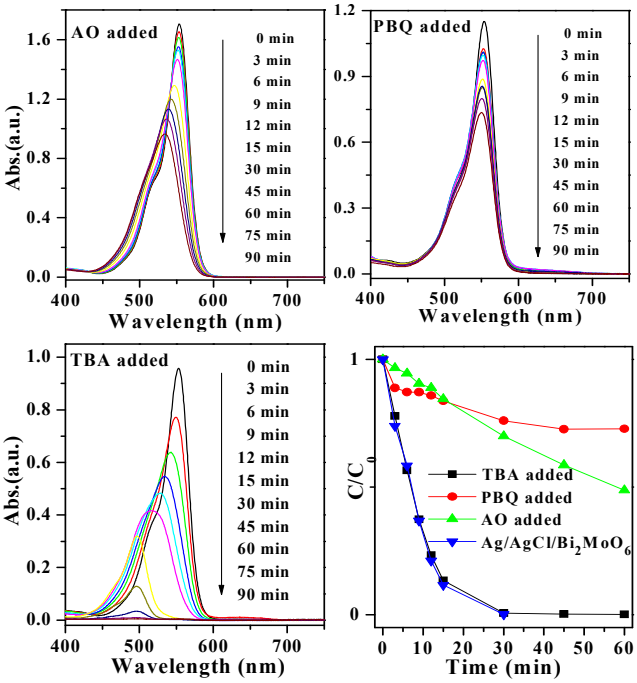

Figure 12. (a) The absorption spectra of RhB in the presence of AAB-30 under exposure to visible light (420 nm < λ < 800 nm) with different active scavenger added, such as AO, PBQ, and TBA.

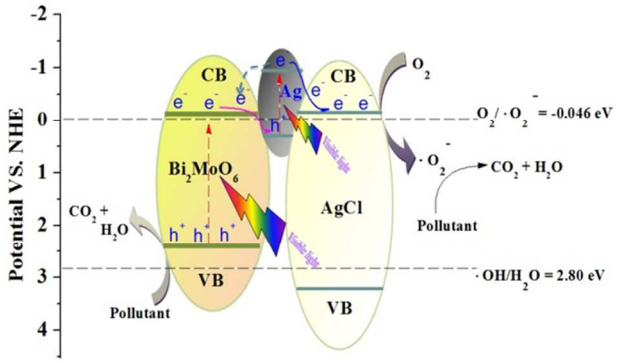

Scheme 1. Photocatalytic degradation mechanism for dyes over $Ag/AgCl/Bi_2MoO_6$ composites under visible light irradiation.

electrons transferred to the surface of AgCl could be further captured by dissolved oxygen to produce $\cdot O_2^-$. Because the CB potential of Bi_2MoO_6 was more negative than that of Ag^+/Ag (+0.799 eV vs NHE), the CB electrons over Bi_2MoO_6 should transfer to the VB of metallic Ag and captured by the holes generated, leaving the VB holes generated over Bi_2MoO_6 directly to react with surface absorbed pollutants.

Conclusions

Novel visible-light responsive $Ag/AgCl/Bi_2MoO_6$ plasmonic photocatalyst was successfully fabricated through a two-step synthesis method. After combination of Ag/AgCl, the $Ag/AgCl/Bi_2MoO_6$ photocatalyst possessed a significantly enhanced visible light activity in decomposing dyes. The highest degradation efficiency was observed for the AAB-30 sample. The activity enhancement was mainly attributed to the SPR effect of Ag^0, and high separation efficiency of electron–hole pairs on their heterojunction interfaces. A possible photocatalytic

degradation mechanism was proposed based on the band potentials of Ag/AgCl and Bi_2MoO_6. This method was expected to be extended for other Ag/AgCl loaded materials, which might have potential applications in removing pollutants.

Acknowledgment

This work was financially supported by the Scientific Research Reward Fund for Excellent Young and Middle-Aged Scientists of Shandong Province (BS2012HZ001), National Natural Science Foundation of China (No. 21103069, 21075052, 21175057, and 40672158), and Scientific Research Foundation for Doctors of University of Jinan (XBS1037 and XKY1043).

References

1 H.B. Wu, H.H. Hng and X.W. Lou, *Adv. Mater*., 2012, **24**, 2567.
2 P. Wang, B. Huang, X. Qin, X. Zhang, Y. Dai, J. Wei and M.H. Whangbo, *Angew.Chem. Int. Ed*., 2008, **47**, 7931.
3 W. Zhou, Z. Yin, Y. Du, X. Huang, Z. Zeng, Z. Fan, H. Liu, J. Wang and H. Zhang, *Small*, 2013, **9**, 140.
4 Y. Bi, H. Hu, S. Ouyang, Z. Jiao, G. Lu and J. Ye, *J. Mater. Chem*., 2012, **22**, 14847.
5 Y. Ou, J. Lin, S. Fang and D. Liao, *Catal. Comm*., 2007, **8**, 936.
6 B. Jiang, C. Tian, Q. Pan, Z. Jiang, J.Q. Wang, W. Yan and H. Fu, *J. Phys. Chem. C*, 2011, **115**, 23718.
7 S. Liu, J. Yu and M. Jaroniec, *J. Am.Chem. Soc*., 2010, **132**, 11914.
8 X. Chen, L. Liu, P.Y. Yu and S.S. Mao, *Science*, 2011, **331**, 746.
9 X. X. Yao and X. H. Liu, *J. Hazard. Mater.*, 2014, **280**, 260.
10 R. Dong, B. Tian, C. Zeng, T. Li, T. Wang and J. Zhang, *J. Phys. Chem. C*, 2013, **117**, 213.
11 C. An, S. Peng and Y. Sun, *Adv. Mater*., 2010, **22**, 2570.
12 Z.W. Seh, S. Liu, M. Low, S.Y. Zhang, Z. Liu, A. Mlayah and M.Y. Han, *Adv. Mater*., 2012, **24**, 2310.
13 X.X. Yao and X.H. Liu, *J. Mol. Catal. A Chem.*, 2014, **393**, 30.
14 L. Han, P. Wang, C. Zhu, Y. Zhai and S. Dong, *Nanoscale*, 2011, **3**, 2931.
15 P.A. DeSario, J.J. Pietron, D.E. DeVantier, T.H. Brintlinger, R.M. Stroud and D.R. Roli-son, *Nanoscale*, 2013, **5**, 8073.
16 M. Zhu, P. Chen, W. Ma, B. Lei and M. Liu, *ACS Appl. Mater. Interfaces*, 2012, **4**, 6386.
17 Y. Tang, Z. Jiang, G. Xing, A. Li, P.D. Kanhere, Y. Zhang, T.C. Sum, S. Li, X. Chen, Z. Dong and Z. Chen, *Adv. Funct. Mater*., 2013, **23**, 2932.
18 P. Wang, B. Huang, X. Qin, X. Zhang, Y. Dai, J. Wei and M.H. Whangbo, *Angew. Chem. Int. Ed*., 2008, **47**, 7931.
19 Y. Bi and J. Ye, *Chem. Commun*., 2009, **43**, 6551.
20 D. Chen, T. Li, Q. Chen, J. Gao, B. Fan, J. Li, X. Li, R. Zhang, J. Sun and L. Gao, *Nanoscale*, 2012, **4**, 5431.
21 J. Hou, C. Yang, Z. Wang, Q. Ji, Y. Li, G. Huang, S. Jiao and H. Zhu, *Appl. Catal. B*, 2013, **142-143**, 579.
22 J. Hou, Z. Wang, C. Yang, W. Zhou, S. Jiao and H. Zhu, *J. Phys. Chem. C*, 2013, **117**, 5132.
23 L.S. Zhang, K.H. Wong, Z.G. Chen, J.C. Yu, J.C. Zhao, C. Hu, C.Y. Chan and P.K. Wong, *Appl. Catal., A: Gen.*, 2009, **363**, 221.
24 H.F. Cheng, B.B. Huang, P. Wang, Z.Y. Wang, Z.Z. Lou, J.P. Wang, X.Y. Qin, X.Y.Zhang and Y. Dai, *Chem. Commun.*, 2011, **47**, 7054.
25 Y. Shimodaira, H. Kato, H. Kobayashi and A. Kudo, *J. Phys. Chem. B*, 2006, **110**, 17790.
26 J. Zhang, C. G. Niu, J. Ke, L. F. Zhou, G. M. Zeng, *Chem. Commun*., 2015, **59**, 30.
27 X. Zhao, J.H. Qu, H.J. Liu and C. Hu, *Environ. Sci. Technol*., 2007, **41**, 6802.
28 Y.H. Zheng, L.R. Zheng, Y.Y. Zhan, X.Y. Lin, Q. Zheng, K.M. Wei, *Inorg. Chem*., 2007, **46**, 6980.
29 D.D. Lin, H. Wu, R. Zhang, W. Pan, *Chem. Mater.*, 2009, **21**, 3479.
30 W.W. Lu, S.Y. Gao, J.J. Wang, *J. Phys. Chem. C*, 2008, **112**, 16792.
31 T. Watanabe, T. Takizawa and K. Honda, *J. Phys. Chem*., 1977, **81**, 1845.
32 T. Takizawa, T. Watanabe and K. Honda, *J. Phys. Chem.*, 1978, **82**, 1391.
33 W.S. Wang, H. Du, R.X. Wang, T. Wen and A.W. Xu, *Nanoscale*, 2013, **5**, 3315.
34 J.D. Zhuang, W.X. Dai, P. Liu, *Langmuir*, 2010, **26**, 9686.
35 Y.H.Liang, S.L. Lin, L. Liu, J.S. Hu, W.Q. Cui, *Appl. Catal. B: Environ.,* 2015, **164**, 192.
36 Y. Yang, W. Guo, Y. Guo, Y. Zhao, X. Yuan and Y. Guo, *J. Hazard. Mater.*, 2014, **271**, 150.
37 X.X. Yao and X.H. Liu, *J. Hazard. Mater.*, 2014, **280**, 260.